Surface & Coatings Technology 205 (2011) 3600–3606

Contents lists available at ScienceDirect

Surface & Coatings Technology

journal homepage: www.elsevier.com/locate/surfcoat

The influence of the deposition parameters on the properties of an rf-magnetron-deposited nanostructured calcium phosphate coating and a possible growth mechanism

Roman A. Surmenev [a,*], Maria A. Surmeneva [a], Kirill E. Evdokimov [a], Vladimir F. Pichugin [a], Thorsten Peitsch [b], Matthias Epple [b]

[a] Department of Theoretical and Experimental Physics, The Centre of Technology, Tomsk Polytechnic University, 634050 Tomsk, Russia
[b] Inorganic Chemistry and Center for Nanointegration Duisburg-Essen (CeNIDE), University of Duisburg-Essen, 45117 Essen, Germany

ARTICLE INFO

Article history:
Received 4 August 2010
Accepted in revised form 22 December 2010
Available online 31 December 2010

Keywords:
rf-magnetron sputtering
Calcium phosphate
Hydroxyapatite
Implant materials

ABSTRACT

The deposition of a biocompatible calcium phosphate coating on the surface of materials for biomedical implants by rf-magnetron sputtering is reported. The deposition parameters to prepare either stoichiometric crystalline hydroxyapatite or amorphous calcium phosphate coating with a molar Ca/P ratio from 1.53 to 3.88 were established. Crystalline hydroxyapatite coating with a Ca/P ratio of 1.60 ± 0.07 can be deposited if the rf-power density is 0.49 W cm^{-2} and if the samples are arranged within the area of the target erosion zone. A thorough investigation of the influence of rf-power, DC-bias on the substrate, deposition time on the properties of the calcium phosphate coating allowed to formulate a mechanism for the film growth.

1. Introduction

Metallic implants are used in surgery to treat bone defects or to replace hard tissue. In principle, all metallic implants are subject to corrosion and mechanical wear after implantation. Often, it is difficult to achieve a strong mechanical interlocking between the implant and the surrounding bone, and a potential risk for implant rejection exists [1]. A metallic implant with a biocompatible coating, such as calcium phosphate, allows the combination of the good mechanical properties of the metal and the good biological properties of the biocompatible coating. This improves the ability of an implant to be integrated with the host tissue. The most frequently used techniques to prepare biocompatible coatings are plasma spraying [2, 3], magnetron sputtering [4–6], biomimetic crystallization techniques [7–9], electrophoretic deposition [10–12], and sol-gel syntheses [13]. For metallic implants made of stainless steel, titanium alloys (Ti6Al4V) or nickel–titanium (NiTi), it is beneficial to coat their surface to prevent the release of heavy metal ions (like nickel) from the surface of the metallic substrate [14] into the surrounding tissue [15, 16]. Therefore, such coatings should be dense, pore-free, biostable, and have a high strength of adhesion to the substrate [6, 14, 17].

Calcium phosphate coatings deposited by radio-frequency (rf) magnetron sputtering can fulfill the aforementioned requirements [18–29]. In order to predict the behavior of an implant in the biological environment, nature and composition of the coating must be known and well defined. This in turn requires a detailed knowledge of the deposition mechanism. Unfortunately, there is still no definite understanding of the mechanisms of the film growth with desired properties, in particular with respect to the calcium to phosphate ratio (Ca/P). However, it is known that in rf-magnetron sputtering deposition parameters like an additional negative electrical bias on the substrate, the working gas atmosphere, the rf-power, the substrate position relative to the erosion zone of the target may all affect the coatings properties [30–32]. Therefore we have carried out a thorough investigation of the target and plasma composition as well as the properties of the calcium phosphate coating deposited by means of rf-magnetron sputtering under variable negative bias, deposition time and position of the substrate relative to the target erosion zone.

2. Materials and methods

A modified commercially available installation 08PKHO-100T-005 (Russia) for plasma etching with an rf-magnetron source (5.28 MHz) was used to deposit the calcium phosphate coatings. A synthetic stoichiometric hydroxyapatite powder, $Ca_{10}(PO_4)_6(OH)_2$, was used as precursor for the target preparation. The powder was pressed and then sintered in air at 1100 °C for 1 h to form the target. The initial structure and stoichiometry of hydroxyapatite were preserved during that process, including the molar Ca/P ratio of 1.67 ± 0.02. The different parameters of the coating deposition are comprised in

* Corresponding author. Tel.: +7 903 953 09 69.
E-mail address: surmenev@tpu.ru (R.A. Surmenev).

0257-8972/$ – see front matter © 2010 Elsevier B.V. All rights reserved.
doi:10.1016/j.surfcoat.2010.12.039

Table 1
Deposition procedures used in the preparation of the calcium phosphate films.

Substrate bias (V)	Deposition time (min)	Average power density at the rf-power 30 W (W cm^{-2})		Average power density at the rf-power 290 W (W cm^{-2})	
		Position 1	Position 2	Position 1	Position 2
Grounded; -50; -100	15; 30; 120; 180	0.051	0.04	0.49	0.38

Table 1. The working gas (Ar) pressure (0.1 Pa; the chamber was evacuated before the experiment to 10^{-4} Pa) and the distance between target and substrate (40 mm) were kept constant in all experiments.

It is well-known that the configuration of the confining magnetic field strongly affects the sputtering characteristics of a planar magnetron. This non-uniformity is responsible for the existence of the cathode erosion profile and the distribution of plasma density. Therefore, the geometry of the samples position is of crucial importance for the properties of the calcium phosphate coating. We defined two sample positions with respect to the target erosion zone: "within" (Position 1) and "out of" (Position 2) (Fig. 1). The average power density ω absorbed by the substrate in these two zones was estimated by assuming that the energy flux is distributed uniformly along the plasma torus and normal to its surface. The calculation of an average power density on the substrate takes into account the area and the angular size of the zones under consideration (see Fig. 1 and Table 1).

It is essential to emphasize that the coatings deposited at position 1 are exposed to more severe ion bombardment in comparison to those deposited at position 2 because the ions move predominantly perpendicular to the substrate. An increased negative bias on the substrate increases the energy of the bombarding ions.

The surface morphology was studied by scanning electron microscopy (SEM) with an ESEM Quanta 400 FEG instrument from FEI, equipped with energy-dispersive X-ray analysis (EDX; EDS analysis system Genesis 4000, SUTW-Si(Li) detector), and operating in high vacuum. The samples were coated with gold/palladium before the SEM study. The EDX spectra were collected for 60 s with a dead time of 30%, the distance between the samples and the source of electrons was 10 mm, and the energy of the electron beam was 10 keV. The coating thickness was measured by embedding the sample, cutting and grinding and direct observation in the SEM (cross-section images). Titanium and silicon were used as substrates. Infrared spectroscopy (IR) was carried out with a Bruker Vertex 70 FTIR instrument (substrates: silicon and potassium bromide pellets). The chemical composition of the plasma was investigated by optical emission spectroscopy (OES) with a spectrometer Avaspec 3648 manufactured by Avantes. The OES spectra were measured in the spectral region 200–860 nm. Identification of the plasma emission lines was performed according to Refs. [33, 34].

X-ray diffractometry was carried out with a Siemens D 500 diffractometer operating with Cu K_α radiation ($\lambda = 1.5406$ Å) at 40 kV and 30 mA in Bragg–Brentano mode. The hydroxyapatite pattern (#9-0432) from the ICDD database was used as reference.

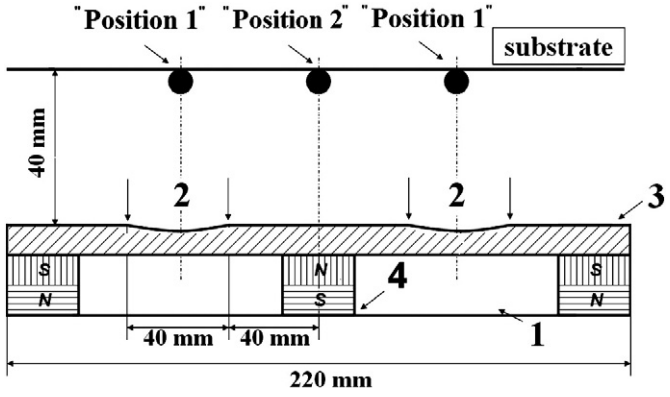

Fig. 1. Schematic representation of the sample position and the cross-section of the magnetron device. **Position 1** corresponds to the substrate position "within" the erosion zone of the target; **Position 2** corresponds to the substrate position "out of" the erosion zone of the target. **1**: cooling system, **2**: target erosion zone; **3**: hydroxyapatite target; **4**: system of magnets (not drawn to scale).

3. Experimental results

3.1. Composition and structure of the hydroxyapatite target

The hydroxyapatite target was characterized by IR spectroscopy, X-ray powder diffraction (Fig. 2) and EDX spectroscopy. All IR absorption bands attributed to hydroxyapatite were present [35], i.e. phosphate ions PO_4^{3-} at 1031 cm^{-1} (ν_3), 1088 cm^{-1} (ν_3), 962 cm^{-1} (ν_1), 601 cm^{-1} (ν_4), 570 cm^{-1} (ν_4) and hydroxide O-H (3571 and 631 cm^{-1}). The target consisted of crystalline hydroxyapatite (Fig. 2b). No peaks attributed to other calcium phosphates or to calcium oxide were found. By EDX, only the elements calcium, phosphorus, oxygen were found, and the Ca/P ratio was 1.67 ± 0.02.

3.2. Plasma composition by optical emission spectroscopy (OES)

Representative light emission spectra from the rf-magnetron sputtering plasma discharge obtained *in situ* are shown in Fig. 3. We found the lines attributed to the working gas, the molecular ions CaO^+, PO_4^{3-}, and the cations Ca^+ and O^+. Klein et al. [19] investigated OES spectra during the sputtering of a hydroxyapatite target and

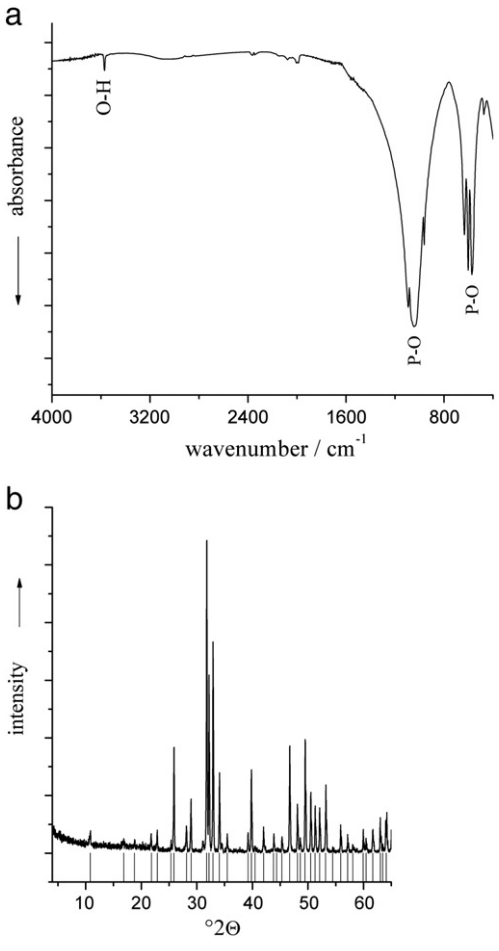

Fig. 2. a) IR spectrum (as KBr pellet) and b) X-ray diffraction pattern of the hydroxyapatite target. The peak positions for hydroxyapatite are marked by vertical lines.

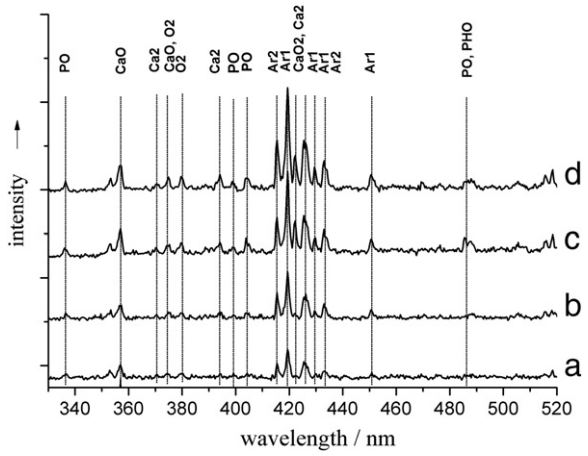

Fig. 3. Representative optical emission spectra measured during the deposition process in argon atmosphere at a pressure of 0.1 Pa. a, b: 30 W, c, d: 290 W. a, c: Negative bias -50 V; b, d: grounded substrate.

found that the content of calcium and phosphorus within the coating depended on the presence of molecular ions such as CaO^+, PO_4^{3-} and cations Ca^+ in the plasma.

An increase in the negative bias on the substrate led to an increase in intensity of emission lines. This is in a good agreement with the results of ref. [36] where a negative bias resulted in an increase in the emission line intensity when using a hydroxyapatite target.

3.3. Substrate temperature

The substrate was heated under the influence of the plasma. The temperature of the substrate was controlled in each deposition run with chromel-copel thermocouples which were put close to the samples near the deposition areas (position 1 and position 2). The substrate temperature as a function of deposition time and rf-power is shown in Fig. 4.

Approximately 50 min was necessary to reach a steady-state at 30 W rf-power and approximately 30 min at 290 W. The equilibrium temperature was 152 ± 6 °C ($\approx$425 K) at 30 W and 300 ± 7 °C ($\approx$573 K) at 290 W.

The substrate temperature did not depend on the substrate bias applied. The substrate temperature was higher when the samples were arranged on the substrate at position 1 in comparison to position 2, because the substrate area within the position 1 (Fig. 1) was more effectively subjected to the plasma heating, i.e. bombardment with ions, electrons and energetic neutral particles.

3.4. Morphology of the calcium phosphate coating

The surface of rf-magnetron deposited coatings was homogeneous, dense, and no cracks were observed (Fig. 5a and c). In Fig. 5b and d, the grains size distributions are presented. The surface morphology can be described as a set of sphere-like islands. A negative bias caused no significant changes in the coating morphology. SEM showed that at early stages (after 15 min deposition time), the calcium phosphate coating already fully covered the substrate surface.

The grain size distribution was obtained by a linear intercept method: The intercepts of a similar length were plotted in each figure with a length of approximately 250 nm. Then the number of the intercepts cross points with the grains boundaries was calculated using Photoshop 10 Professional. The grain size was calculated as a ratio of the mean intercept length to the mean quantity of cross points. The average grain size at a rf-power level of 290 W was 65 nm (position 2, Fig. 5a) after 15 min of deposition. At an rf-power of 30 W, the average grain size was approximately 10 nm, and no significant difference was observed between positions 1 and 2. When the deposition time was increased to 180 min, the average grain size increased to 105 nm at position 2 at 290 W (Fig. 5c); if a power of 30 W was applied, the average grain size increased to 30–40 nm both at position 1 and 2.

3.5. Elemental composition of the calcium phosphate coatings

EDX showed that the elemental composition of the coatings corresponded to the target composition and did not depend on the chosen deposition procedure. The ratio of the elements in the coating, in particular the Ca/P ratio, depended on the applied rf-power, the negative substrate DC-bias, and the power density on the substrate position. The experimental values of the Ca/P ratio in the formed structures under different deposition parameters are given in Table 2.

The Ca/P ratio depended on the thickness of the coating. Moreover, an increase in the negative bias at rf-power of 30 W almost doubled the Ca/P ratio (Table 2), whereas in the case of 290 W the change of Ca/P ratio with the bias voltage was almost insignificant. Therefore, the increase in the rf-power reduced the effect of the negative bias considerably (Table 2). The Ca/P ratio in the coating deposited at rf-power of 290 W on the position 2 was higher compared to that on the position 1 in all cases.

A growth of the coating thickness was accompanied with a decrease in Ca/P ratio as it was also reported in ref. [23]. Feddes et al. explained this phenomenon by assuming that phosphorus was resputtered from the growing film surface by negative oxygen ions with the energy determined by the potential drop in the cathode dark sheath. The source of the oxygen ions is the hydroxyapatite target. Measurements of the voltage drop in the cathode dark sheath with a voltmeter that was built in the feedback of rf-generator allowed the estimation the maximum energy of single negative oxygen ions that are accelerated in the cathode dark sheath of 170 eV at an rf-power 30 W and up to 315 eV at an rf-power of 290 W. A resputtering phenomenon of a growing film by the negative oxygen ions with energies equivalent to the cathode dark sheath drop was also reported in the literature for other oxide targets, namely $YBa_2Cu_3O_{7-x}$, $Ta_2Zn_3O_8$ and α-Al_2O_3 [37–40].

3.6. The calcium phosphate coating phase composition and molecular structure

The coating deposited at 30 W was fully X-ray amorphous. The peaks that are typical for crystalline hydroxyapatite appeared only after 180 min of the deposition.

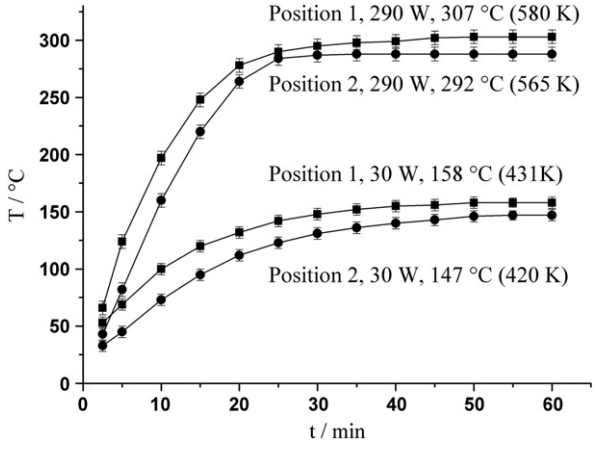

Fig. 4. Substrate temperature at different positions versus deposition time. Rf-power was set to 290 or 30 W.

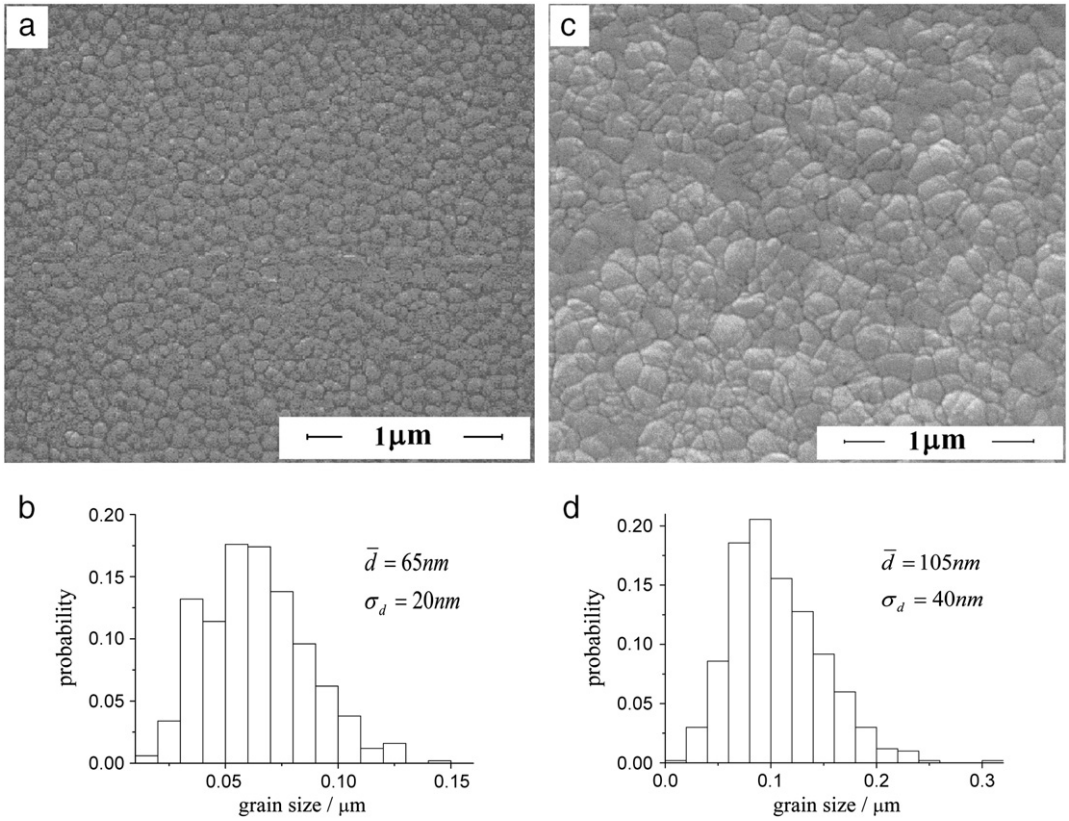

Fig. 5. SEM-patterns of calcium phosphate coating morphology deposited at 290 W, position 2 (a: deposition time 15 min; c: deposition time 180 min), grounded substrate (silicon wafer). b and d: Corresponding histograms of the grain size distribution. $\bar{d}$ is the average grain size, and σ is the standard deviation.

An rf-power level of 290 W resulted in an amorphous coating after 30 min of the deposition. When the deposition time was increased from 30 to 180 min (Fig. 6) the crystallization of the coating to the hydroxyapatite with a preferred crystallographic (002) orientation occurred [6]. Peaks at 25.8° (002), 53.1° (004), 31.8° (211), 32.2° (112), and 32.9° (300) appeared, but the last three peaks overlapped, all in agreement with literature data [4, 27, 36, 41, 42]. Besides the peaks assigned to crystalline hydroxyapatite, no peaks of other calcium phosphates like tricalcium phosphate, tetracalcium phosphate or of calcium oxide were found.

IR spectra showed the presence of absorption bands typical for hydroxyapatite (Fig. 7). However, a change in the band characteristics (amplitude, width at half height) occurred that was caused by changes in the surrounding of the PO_4^{3-} ions in the lattice of hydroxyapatite and reorientation of the crystallites within the coating. This is proved by the experimental data presented in Table 2. In the IR spectra, the bands assigned to the valence and deformative vibrations of the ions PO_4^{3-} at 570 cm^{-1} (ν_4), 601 cm^{-1} (ν_4) and 1031 cm^{-1} (ν_3) [43–46] were found. The bands of O-H ions in the deposited coatings were only weakly resolved at 631 and 3571 cm^{-1},

Table 2
The molar Ca/P ratio of the coatings as a function of the deposition parameters as determined by EDX. The error was within 0.02 to 0.05. The bias of 0 V corresponds to the grounded substrate. * Ca/P change relative to the grounded substrate.

rf-power (W)	Time (min)	Bias (V)	Position 1			Position 2		
			Thickness (nm)	Ca/P	Ca/P change*	Thickness / nm	Ca/P	Ca/P change*
290	30	0	120±20	2.15	–	140±20	2.41	–
		-50	105±20	2.19	+0.04	130±20	2.5	+0.09
		-100	100±20	2.4	+0.25	120±20	2.79	+0.38
	120	0	520±30	1.67	–	650±30	1.87	–
		-50	560±30	1.76	+0.09	670±30	1.96	+0.09
		-100	650±30	1.86	+0.19	690±30	1.98	+0.11
	180	0	820±30	1.58	–	980±30	1.9	–
		-50	880±30	1.53	-0.05	1030±30	1.89	-0.01
		-100	990±30	1.57	-0.01	1060±30	1.92	+0.02
30	30	0	20±15	2.01	–	25±15	2.02	–
		-50	20±15	2.50	+0.49	25±15	2.45	+0.43
		-100	20±15	3.88	+1.87	25±15	3.05	+1.03
	120	0	100±20	1.86	–	115±20	2.03	–
		-50	75±20	2.25	+0.39	105±20	2.48	+0.45
		-100	70±20	3.62	+1.76	95±20	3.0	+0.97
	180	0	145±20	1.84	–	160±20	1.72	–
		-50	135±20	2.12	+0.28	150±20	2.2	+0.48
		-100	95±20	3.41	+1.57	140±20	2.44	+0.72

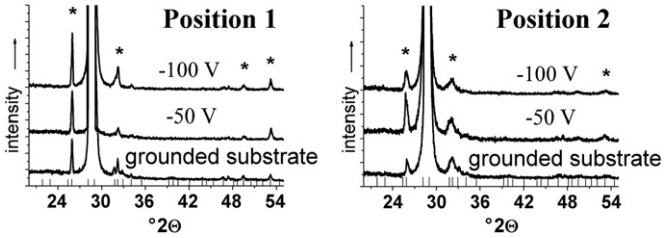

Fig. 6. XRD patterns of the calcium phosphate coating deposited at 290 W for 180 min on a silicon wafer. "*" denotes the peaks attributed to hydroxyapatite. The vertical lines show the peaks of hydroxyapatite (ICDD card number 09-432).

indicating that a part of the ions OH^- was lost during target sputtering. The coating structure in this case corresponds to the dehydroxylated hydroxyapatite with the chemical formula $Ca_{10}(PO_4)_6(OH)_{2-2x}O_xV_x$, where V denotes a vacancy ($0<x<1$).

Thus, the analysis of elemental composition of the coatings by X-ray diffraction and IR spectroscopy showed that a coating of crystalline and stoichiometric hydroxyapatite (Ca/P = 1.67) can be obtained at an rf-power of 290 W at a power density of 0.49 W cm^{-2} that corresponds to position 1 (see Table 2).

The analysis of the elemental composition and the coating structure revealed that an excess of calcium in the coating (Ca/P of 1.67–3.88) can be explained by the presence of amorphous calcium oxide (besides the main phase of hydroxyapatite) as it was also reported in ref. [36]. The deposition procedures with Ca/P in the range of 1.53–1.67 resulted in a coating with a structure close to calcium-deficient hydroxyapatite with the chemical formula $Ca_{10-x}(HPO_4)_x(PO_4)_{6-x}(OH)_{2-x}$ where $0<x<1$ [47]. The formation of the coating with this structure was dependent on the deposition conditions and occurred at the maximum ions bombardment rate (position 1). This is connected with the resputtering of calcium from calcium oxide that is not strongly bound to the main phase of the coating. Resputtering of calcium in the case of the coating deposited on position 2 was less effective, therefore after 180 min of the deposition at an rf-power of 290 W, the Ca/P ratio was in the range of 1.89–1.92; at the same time at position 1, the Ca/P ratio was in the range of 1.53–1.58 (Table 2).

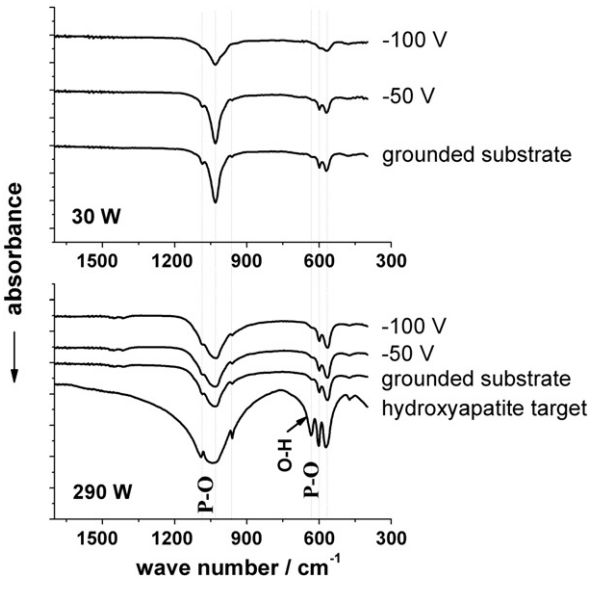

Fig. 7. IR spectra of the calcium phosphate coating on KBr single crystal substrate with a deposition time of 180 min in position 1.

3.7. A possible mechanism for the growth of calcium phosphate coatings from rf-plasma discharge

The change in the Ca/P ratio in the films prepared during different deposition time can be explained either by alteration of the anode dark sheath voltage drop caused by the growing dielectric calcium phosphate coating or by changes in the coating characteristics themselves. The analysis of the processes at substrate surface adjacent to plasma and anode dark sheath allows the assumption that the following sequence of processes leads to the formation of calcium phosphate coating:

1) The ignition of the rf-discharge creates a flux of ions and neutral atoms (atomic clusters) directed to the growing film which initiates the coating growth process. The composition of this flux is identical to that of the target material.
2) An external electrical bias applied to the substrate creates an electric field in the anode dark sheath. The electric field accelerates positively charged ions (Ca^+, CaO^+, HPO^+ and others) towards the substrate. The higher the applied negative bias, the higher is the kinetic energy of the ions that bombard the substrate.
3) The electric field strength does not depend on time; therefore the energy distribution of positively charged ions bombarding the surface does not depend on time either.
4) The particles from plasma form a layer of adatoms on the substrate surface. Resputtering of the atoms from the growing coating is a competitive process.
5) The coating structure is amorphous at the initial stage of deposition. At this stage, there is an enrichment in calcium due to more effective resputtering of phosphorus atoms from the amorphous coating. This leads to a higher Ca/P ratio (1.76–3.88) in the coating in comparison to stoichiometric hydroxyapatite (1.67).
6) An increase in the deposition time causes heating and crystallization of the coating that leads to a decrease in the probability of phosphorus resputtering and preferable of resputtering excess calcium atoms. This decreases the Ca/P ratio.

The value of electric field strength in anode dark sheath depends on the electric charge and the geometric configuration of the considered system. Plasma and uncompensated charge on the coating surface create an electric field within the anode dark sheath. The strength of this electric field is negligible in comparison to that created by the bias voltage applied. Therefore, the electric charge both in anode dark sheath and in the volume of the dielectric coating can be neglected.

In order to estimate the electric field strength it was assumed that the plasma is an ideal conductor and that the dielectric coating is uniform and isotropic. The width of the anode dark sheath is much smaller than other characteristic sizes of experimental setup. Hence, the local situation is equivalent to a plane capacitor with a vacuum gap partially filled with a plane dielectric.

The resulting geometry is one-dimensional (Fig. 8). The electric potential distribution is determined by the Poisson equation $\Delta U_{1,2}=0$ with U_1 and U_2 the electric potential in the anode dark sheath and dielectric coating, respectively. The boundary conditions are $U_1(-\lambda_{sh})=V_1$, $U_2(d_2)=V_2$, $U_1(0)=U_2(0)$, $U'_1(0)=\varepsilon U'_2(0)$, with λ_{sh} the anode dark sheath width, d_2 the dielectric coating thickness, ε the dielectric constant of the coating, and V_1, V_2 the electric potential of plasma and substrate, respectively. The zero value of the space variable corresponds to the vacuum-dielectric coating interface. The solution of the Poisson equation gives the dependence of electric field strength (E_1) on the voltage in the anode dark sheath:

$$E_1 = \Delta V / (d_2 / \varepsilon + \lambda_{sh}) \quad (1)$$

with $\Delta V = (V_2 - V_1)$ the potential drop in anode dark sheath.

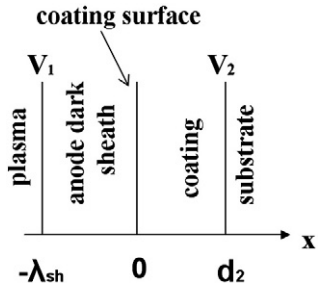

Fig. 8. The arrangements of electrodes for estimation of the influence of the calcium phosphate coating thickness on the electric field distribution in the anode dark sheath.

The anode dark sheath thickness λ_{sh} was estimated according to refs. [48, 49]:

- in the case of a grounded substrate holder

$$\lambda_{sh} = \gamma \cdot \lambda_d = \gamma\sqrt{\varepsilon_0 T_e / (en_p)} \quad (2)$$

- in the case of a high bias, *i.e.* $V_s >> T_e$

$$\lambda_{sh} = (\sqrt{2}/3)\lambda_d (2V_s/T_e)^{\frac{3}{4}} \quad (3)$$

with V_s the bias voltage, n_p the plasma density, T_e the electron temperature of the plasma, λ_d the Debye length, $\gamma = 1$–5. Eq. (3) is valid under the following conditions: $\Delta V \geq 50$ V, $n_p = (10^{14}$–$10^{18})$ m^{-3}, and $T_e = (1$–$10)$ eV [4].

The estimation of plasma density was carried out according to molecular kinetic theory. At the given deposition parameters ($p = 0.1$ Pa; $T_{ions} = 293$ K), the density of working gas atoms is estimated to $n = 10^{19}$ m^{-3}. Taking into account a low level of ionization of plasma (0.0001–0.001), the density of ions in the plasma is $(10^{15}$–$10^{16})$ m^{-3}. These values are in accordance with the data reported in ref. [49]. The electron temperature T_e within a plasma is in the range of (1–10) eV [4, 48, 50]. The estimation of the minimal width of the anode dark sheath with the applied study deposition parameters gave 74 μm. The presence of a dielectric coating significantly influences the electric field strength in the anode dark sheath if the condition $d_2/\varepsilon \approx \lambda_{sh}$ is fulfilled. The substitution of a maximum value of the coating width of 2.7 μm prepared in this study and $\varepsilon_{CaO} = 11.38$ [34] allowed to derive the upper threshold of the d_2/ε ratio to be 0.247 μm, *i.e.* $d_2/\varepsilon << \lambda_{sh}$. Thus, a dielectric coating deposited on the substrate does not affect the electric field in anode dark sheath at the given deposition parameters. Furthermore, the flux of ions from plasma towards the growing film is constant during the deposition run. It does not depend on the thickness of the dielectric calcium phosphate film and depends only on the deposition parameters.

Negatively charged ions within the plasma affect the deposition process if the energy of the ions at the plasma boundary exceeds their loss of energy in anode dark sheath, i.e.

$$kT_e \geq 2q\Delta V \quad (4)$$

with q the ion charge and k the Boltzmann constant.

According to Eq. (4), the negative single-charged phosphorus-containing ions can reach the substrate if their thermal energy exceeds 200 eV. The thermal energy of ions in the plasma is significantly smaller than this value, therefore they cannot reach the substrate [48]. Thus, the main building components of the calcium phosphate coating are positive ions, neutral atoms and clusters of atoms (Fig. 3).

The thorough analysis of the experimental results and processes of calcium phosphate coating growth from rf-magnetron discharge allows to summarize the obtained results. When a low plasma power density is applied (30 W), no crystallization occurs due to less energy intake and the calcium phosphate coating remains amorphous. A rise of bias voltage results in an increase in the Ca/P ratio due to more effective resputtering of phosphorus-containing species from the coating surface by bombarding particles. When a high rf-power level is applied (290 W), the coating is amorphous at the initial stages of deposition (15, 30 min). Subsequent crystallization of the coating leads to a decrease in the Ca/P ratio with time due to more effective resputtering of calcium from calcium-containing compounds that are not bound with main phase of the coating (hydroxyapatite).

4. Conclusion

The rf-magnetron deposited calcium phosphate coatings are homogenous, dense, pore-free, and without any defects and cracks. The variation of negative substrate bias, deposition time and rf-power led to coatings with a Ca/P ratio from 1.53 to 3.88 and either crystalline or amorphous structure. A coating of crystalline hydroxyapatite with a Ca/P ratio of 1.60 ± 0.07 can be prepared if an rf-power density of 0.49 W cm^{-2} is applied and if the samples are arranged within the area of the target erosion zone. The proposed mechanism of calcium phosphate coating growth from rf-plasma discharge is in good agreement with the experimental results. It is worth to emphasize that plasma-assisted fabrication is a rather complex process, and to prepare a calcium phosphate film with predetermined properties, both the incoming flux of atoms and the flux of resputtered atoms must be taken into account. The possibility to control the crystallinity of the coating has a direct consequence for the lifetime of the coating *in vivo*: an amorphous coating will be faster resorbed than a crystalline one [51]. This can be chosen according to the desired application, e.g. in bone contact. Of course, a high adhesion strength is of high importance for any biomedical application.

Acknowledgements

The authors thank Mr. S. Boukercha for experimental assistance with SEM experiments.

References

[1] B.D. Ratner, A.S. Hoffman, F.J. Schoen, Biomaterials Science. An Introduction to Materials in Medicine, Academic Press, 2004.
[2] K. de Groot, R. Geesink, C.P.A.T. Klein, P. Serekian, J. Biomed. Mater. Res. 21 (1987) 1375.
[3] L. Sun, C.C. Berndt, K. Gross, A. Kucuk, J. Biomed. Mater. Res. 58 (2001) 570.
[4] I. Levchenko, K. Ostrikov, M. Keidar, S. Xu, J. Appl. Phys. 98 (2005) 064304.
[5] M. Yoshinari, Y. Ohshiro, T. Derand, Biomaterials 15 (1994) 529.
[6] V.F. Pichugin, R.A. Surmenev, E.V. Shesterikov, M.A. Ryabtseva, E.V. Eshenko, S.I. Tverdokhlebov, O. Prymak, M. Epple, Surf. Coat. Technol. 202 (2008) 3913.
[7] A. Stoch, W. Jastrzebski, A. Brozek, J. Stoch, J. Szaraniec, B. Trybalska, G. Kmita, J. Mol. Struct. 555 (2000) 375.
[8] K. Flade, C. Lau, M. Mertig, W. Pompe, Chem. Mater. 13 (2001) 3596.
[9] P. Habibovic, F. Barrère, C.A. van Blitterswijk, K. de Groot, P. Layrolle, J. Am. Ceram. Soc. 85 (2002) 517.
[10] L.A. de Sena, M.C. de Andrade, A.M. Rossi, G.D.A. Soares, J. Biomed. Mater. Res. Appl. Biomater. 60 (2002) 1.
[11] S. Rößler, A. Sewing, M. Stölzel, R. Born, D. Scharnweber, M. Dard, H. Worch, J. Biomed. Mater. Res. 64A (2003) 655.
[12] H. Urch, S. Franzka, D. Dahlhaus, N. Hartmann, E. Hasselbrink, M. Epple, J. Mater. Chem. 16 (2006) 1798.
[13] K.A. Gross, C.S. Chai, G.S.K. Kannangara, B. Ben-Nissan, J. Mater. Sci. Mater. Med. 9 (1998) 839.
[14] R.A. Surmenev, M.A. Ryabtseva, E.V. Shesterikov, V.F. Pichugin, T. Peitsch, M. Epple, J. Mater. Sci. Mater. Med. 21 (2010) 1233.
[15] T. Peitsch, A. Klocke, B. Kahl-Nieke, O. Prymak, M. Epple, J. Biomed. Mater. Res. 82A (2007) 731.
[16] S. Shabalovskaya, J. Anderegg, J. van Humbeeck, Acta Biomater. 4 (2008) 447.
[17] D.V. Shtansky, N.A. Gloushankova, A.N. Sheveiko, M.A. Kharitonova, T.G. Moizhess, E.A. Levashov, F. Rossi, Biomaterials 26 (2005) 2909.

[18] J.A. Jansen, J.G.C. Wolke, S. Swann, J.P.C.M. van der Waerden, K. de Groot, Clin. Oral Impl. Res. 4 (1993) 28.
[19] C.P.A.T. Klein, P. Patsa, J.G.C. Wolke, J. Blieck-Hogervorst, K. de Groot, J. Biomed. Mater. Res. 28 (1994) 909.
[20] J.G.C. Wolke, J.P.C.M. van der Waerden, K. de Groot, J.A. Jansen, Biomaterials 18 (1997) 483.
[21] D. Ruddel, J. Thompson, B.R. Stoner, J. Biomed. Mat. Res. 51 (2000) 316.
[22] V. Nelea, C. Morosanu, M. Iliescu, I.N. Mihailescu, Surf. Coat. Technol. 173 (2003) 315.
[23] B. Feddes, J.G.C. Wolke, J.A. Jansen, A.M. Vredenberg, J. Appl. Phys. 93 (2003) 9503.
[24] E.I. Suvorova, V.V. Klechkovskaja, V.V. Bobrovsky, Y.D. Khamchukov, V.V. Klubovich, J. Crystallogr. Rep. 48 (2003) 872.
[25] S. Xu, J. Long, L. Sim, C.H. Diong, K. Ostrikov, Plasma Proc. Polym. 2 (2005) 373.
[26] E. van der Wahl, J.G.C. Wolke, J.A. Jansen, A.M. Vredenberg, Appl. Surf. Sci. 246 (2005) 183.
[27] A.R. Boyd, B.J. Meenan, N.S. Leyland, Surf. Coat. Technol. 200 (2006) 6002.
[28] Y. Yonggang, J.G.C. Wolke, L. Yubao, J.A. Jansen, J. Biomed. Mater. Res. A 76 (2006) 744.
[29] A.R. Boyd, H. Duffy, R. McCann, M.L. Cairns, B.J. Meenan, Nucl. Instrum. Meth. Phys. Res. 258 (2007) 421.
[30] S.B. Krupanidhi, M. Sayer, J. Appl. Phys. 56 (1984) 3308.
[31] S. Ismat Shah, Bull. Mater. Sci. 14 (1991) 503.
[32] M. Ohring, The Materials Science of Thin Films, Elsevier, 1991.
[33] R.W.B. Pearse, A.G. Gaydon, The Identification of Molecular Spectra, John Wiley&Sons, New York, 1976.
[34] D.R. Lide, CRC Handbook of Chemistry and Physics, 2005,, Internet Version.
[35] P.F. González-Díaz, M. Santos, J. Solid State Chem. 22 (1977) 193.
[36] J. Long, L. Sim, S. Xu, K. Ostrikov, Chem. Vap. Dep. 13 (2007) 299.
[37] J.M. Andersson, E. Wallin, E.P. Münger, U. Helmersson, J. Appl. Phys. 100 (2006) 033305.
[38] T.I. Selinder, G. Larsson, U. Helmersson, S. Rudner, J. Appl. Phys. 69 (1991) 390.
[39] P.D. Rack, M.D. Potter, A. Woodard, S. Kurinec, J. Vac. Sci. Technol. A 17 (1999) 2805.
[40] S.M. Arora, V.H. Desai, K.B. Sundaram, L. Chow, J. Chen, Phys. Stat. Sol. A 126 (1991) 377.
[41] J.E.G. Hulshoff, K. van Dijk, J.P.C.M. van der Waerden, J.G.C. Wolke, W. Kalk, J.A. Jansen, J. Biomed. Mater. Res. 31 (1996) 329.
[42] J.L. Ong, G.N. Raikar, T.M. Smoot, Biomaterials 18 (1997) 1271.
[43] J.L. Ong, L.C. Lucas, Biomaterials 15 (1994) 337.
[44] J. Weng, X.G. Liu, X.D. Li, X.D. Zhang, Biomaterials 16 (1995) 39.
[45] K. van Dijk, H.G. Schaeken, J.G.C. Wolke, J.A. Jansen, F.H.P.M. Habraken, J. Verhoeven, C.H.M. Marée, Surf. Coat. Technol. 76–77 (1995) 206.
[46] K.V. van Dijk, J.C.H.M. Marée, F.H.P.M. Habraken, J.A. Jansen, Thin Solid Films 304 (1997) 191.
[47] S.V. Dorozhkin, M. Epple, Angew. Chem. Int. Ed. 41 (2002) 3130.
[48] M.A. Lieberman, A.J. Lichtenberg, Principles of Plasma Discharges and Materials Processing, John Wiley&Sons, New York, 1994.
[49] I. Levchenko, K. Ostrikov, J. Phys. D Appl. Phys. 40 (2007) 2308.
[50] I. Levchenko, M. Korobov, M. Romanov, M. Keidar, J. Phys. D Appl. Phys. 37 (2004) 1690.
[51] R. Detsch, D. Hagmeyer, M. Neumann, S. Schaefer, A. Vortkamp, M. Wuelling, G. Ziegler, M. Epple, Acta Biomater. 6 (2010) 3223.